Helium breakup states in ^{10}Be and ^{12}Be

M. Freer,[1,2] J. C. Angélique,[2] L. Axelsson,[3] B. Benoit,[4] U. Bergmann,[5] W. N. Catford,[6] S. P. G. Chappell,[7] N. M. Clarke,[1] N. Curtis,[6] A. D'Arrigo,[4] E. de Góes Brennard,[4] O. Dorvaux,[8] B. R. Fulton,[1] G. Giardina,[9] C. Gregori,[10] S. Grévy,[11,*] F. Hanappe,[14] G. Kelly,[12] M. Labiche,[2] C. Le Brun,[2] S. Leenhardt,[11] M. Lewitowicz,[13] K. Markenroth,[3] F. M. Marqués,[2] J. T. Murgatroyd,[1] T. Nilsson,[3,†] A. Ninane,[2,‡] N. A. Orr,[2] I. Piqueras,[10] M. G. Saint Laurent,[13] S. M. Singer,[1] O. Sorlin,[11] L. Stuttgé,[8] and D. L. Watson[14]

[1]*School of Physics and Astronomy, University of Birmingham, Edgbaston, Birmingham B15 2TT, United Kingdom*

[2]*Laboratoire de Physique Corpusculaire, ISMRA and Université de Caen, IN2P3-CNRS, F-14050 Caen Cedex, France*

[3]*Fysiska Institutionen, Chalmers Tekniska Högskola, S-412 96 Göteborg, Sweden*

[4]*Université Libre de Bruxelles, CP 226, B-1050 Bruxelles, Belgium*

[5]*Det Fysiske Institut, Aarhus Universitet, DK 8000 Aarhus C, Denmark*

[6]*Department of Physics, University of Surrey, Guildford, Surrey GU2 5XH, United Kingdom*

[7]*Nuclear and Astrophysics Laboratory, University of Oxford, Keble Road, Oxford OX1 3RH, United Kingdom*

[8]*Institut de Recherches Subatomique, IN2P3-CNRS/Université Louis Pasteur, Boîte Postale 28, F-67037 Strasbourg Cedex, France*

[9]*Istituto Nazionale di Fisica Nucleare, Sezione di Catania and Dipartimento di Fisica, Universitá di Messina, Messina, Italy*

[10]*Instituto Estructura de la Materia, CSIC, E-28006 Madrid, Spain*

[11]*Institut de Physique Nucléaire, IN2P3-CNRS, F-91406 Orsay Cedex, France*

[12]*School of Sciences, Staffordshire University, College Road, Stoke-on-Trent ST4 2DE, United Kingdom*

[13]*GANIL (CEA/DSM-CNRS/IN2P3), BP 5027, F-14076 Caen Cedex, France*

[14]*Department of Physics, University of York, York YO1 5DD, United Kingdom*

(Received 5 June 2000; revised manuscript received 12 September 2000; published 26 January 2001)

The breakup of ^{10,12}Be into He clusters has been studied using the p,^{12}C(^{12}Be,^{6}He,^{6}He) and ^{12}C(^{12}Be,^{4}He,^{6}He) inelastic scattering and two neutron transfer reactions with a 378 MeV ^{12}Be beam incident on ^{12}C and $(CH_2)_n$ targets. Evidence has been found for three new states in ^{10}Be at excitation energies of 13.2, 14.8, and 16.1 MeV, which may be associated with a ^{4}He+^{6}He cluster structure. The evidence for He cluster states in ^{12}Be in the excitation energy range 12 to 25 MeV is also discussed.

DOI: 10.1103/PhysRevC.63.034301 PACS number(s): 21.10.Hw, 25.70.Ef, 21.60.Gx, 27.20.+n

I. INTRODUCTION

The role of the α particle in the structure of light nuclei is well documented, and forms the basis for many successful models. The antisymmetrized alpha cluster model developed in the 1960's [1,2] has since provided a description of the structure and spectroscopy of α-conjugate nuclei spanning the p, sd, and fp shells [3,4]. The success of this model lies in the stability of the ^{4}He nucleus and the relative weakness of the α-α interaction. It might be expected that nuclei not entirely composed of α particles would have their cluster structure diluted. However, the extension of the antisymmetrized alpha cluster model to describe non-α-conjugate systems by Horiuchi and co-workers [5–9] demonstrates that clustering remains in systems composed of collections of α particles and valence nucleons. This framework, called antisymmetrized molecular dynamics (AMD), employs a Slater determinant wave function to model an N-nucleon system with Gaussian forms for the nucleonic wave functions, and *in principle* does not impose clustering prior to the minimization of the binding energy of the system. Nevertheless, cluster structure is apparent in, for example, the calculations for the isotope chains of the elements Be, B, and C [8,9]. The results of this model are not unique as a number of other models, such as the generator coordinate method (GCM) calculations [10–13], have also successfully described the structure of a large number of non-α-conjugate nuclei in terms of a cluster substructure.

Recently, the AMD framework has been used to illustrate the phenomenon of ''molecular-like binding'' on the nuclear scale [5,9]. These ideas were originally developed by Okabe *et al.* [14] and Seya *et al.* [15] to describe the behavior of systems composed of two α particles and valence neutrons or protons. The ^{8}Be nucleus is the archetypal α-cluster nucleus, there being considerable experimental and theoretical evidence to support its two-α structure. Far from being diluted by the addition of further particles, this cluster structure has an important impact on the structure and properties of its neighboring nuclei. The single-particle orbits which arise from the two-centered nature of the ^{8}Be nuclear potential have been described, variously, in terms of a molecular-orbital model [15] and the two center shell model (TCSM) [9,16]. These orbits bear a strong resemblance to those of electrons in the σ and π orbits associated with the covalent binding of atomic molecules. This molecular description can account for the properties of, for example, ^{9}Be which possesses rotational bands indicative of large deformations, built

*Present address: Laboratoire de Physique Corpusculaire, ISMRA et Université de Caen, IN2P3-CNRS, Bd Maréchal Juin, 14050 Caen Cedex, France.

†Present address: ISOLDE, PPE-Division, CERN, CH-1211 Geneve 23, Switzerland.

‡On leave from: Institut de Physique, Université Catholique de Louvain, Louvain-la-Neuve, Belgium.

on the ground and low-lying states which possess molecular-like structures.

These ideas may also be extended to the $\alpha+2n+\alpha$ system ^{10}Be, where the ground state is associated with a compact molecular type structure, but it is the rotational bands built on the $K=0_2^+$, 1^-, 2^-, and 2^+ configurations, all of which have band heads at ~ 6 MeV, in which the molecular structure is most pronounced. A recent survey of the available experimental data by von Oertzen [17–19] suggests that the molecular phenomenon extends to even more neutron-rich nuclei, e.g., ^{11}Be and further to systems composed of more than two α particles. Moreover, a study of the decay of ^{12}Be into helium clusters found evidence for a possible $\alpha+4n+\alpha$ molecular structure [20], originally hinted at in the earlier study of Korsheninnikov *et al.* [21].

Such decay studies provide an important signature for cluster formation, as highly clustered states should possess large partial decay widths for channels asymptotically associated with the corresponding substructure. In the case of ^{10}Be, evidence for $\alpha+^6$He clustering was found in a measurement of the ^{7}Li(^{7}Li,α,^{6}He)α reaction, performed by Soić *et al.* [22]. However, these data were limited to only a very narrow excitation energy region close to the α-decay threshold. The present paper presents a study of the α decay of ^{10}Be states over the much wider excitation energy range 10 to 20 MeV. We also report on the angular distributions and cross sections for the p,^{12}C(^{12}Be,^{6}He,^{6}He) reactions originally presented in Ref. [20].

II. EXPERIMENTAL DETAILS

A 378 MeV ^{12}Be secondary beam, with an energy spread of 18 MeV and intensity 2×10^4 particles per second, was produced from a 63 MeV per nucleon ^{18}O beam of intensity 2 μA, provided by the GANIL coupled cyclotrons. The ^{18}O beam was incident on a thick beryllium fragmentation target. Purification of the secondary beam ($\sim$95% ^{12}Be) was achieved using the LISE3 spectrometer. The secondary beam was tracked onto 10 mg cm^{-2} natural carbon (denoted ^{nat}C) and 37 mg cm^{-2} $(CH_2)_n$ target foils, using two x-y position sensitive parallel plate avalanche counters. These detectors allowed the measurement of the incident angle, position on target and energy of the beam (determined using time of flight techniques) with resolutions of 1°, 1 mm, and 3.5 MeV, full width at half maximum (FWHM), respectively.

The helium breakup products from the ^{12}C(^{12}Be,^{4}He,^{6}He)^{14}C and p,^{12}C(^{12}Be,^{6}He,^{6}He) reactions, on both the $(CH_2)_n$ and ^{nat}C targets, were detected using an array of 10 Si-CsI telescopes. The Si elements were 500 μm thick, 5×5 cm^2 two-dimensional position sensitive detectors. The resolution with which the position of the incident particles could be measured was $\sim$2 mm (FWHM). These were backed by 4.0 cm thick CsI detectors with a photodiode readout, providing a measurement of energy of the incident ions with a resolution of 1.5% (FWHM). The detectors were arranged in a symmetric fashion around the beam axis so as to pick up breakup fragments in opposite telescopes. The array spanned the full range of azimuthal angles and polar angles from 2° to 24° in the laboratory frame of reference.

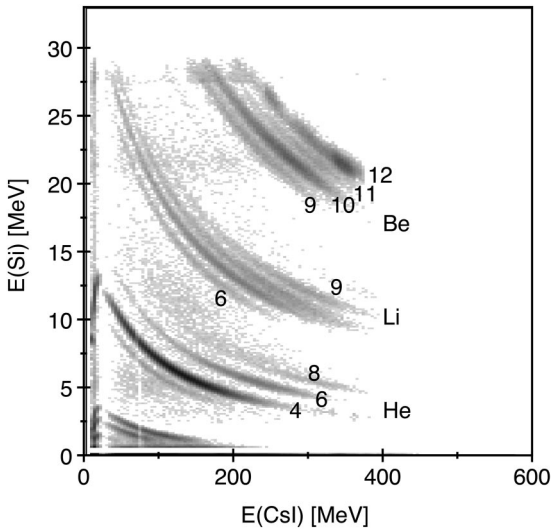

FIG. 1. Particle identification spectrum for the silicon-CsI telescopes.

The silicon detectors were calibrated using α-source measurements, and the CsI detectors were calibrated using a mixed secondary beam from LISE containing species from ^{4}He to ^{12}Be. This combination of isotopes allowed the characteristic light emission profiles to be calibrated for a variety of ion species. The light response, f(light), was then modeled for each incident ion with charge Z, mass A and energy E using the characteristic function [23]

$$f(\text{light}) = a_0 + a_1\left(E - a_3AZ^2\ln\left[\frac{E+a_2AZ^2}{a_2AZ^2}\right]\right). \quad (1)$$

The coefficients a_0, a_1, a_2, and a_3 extracted from the analysis of the calibration data were used to predict the pulse height from the preamplifier associated with the photodiode readout of each CsI crystal for each incident fragment, and hence provided a method for reconstructing the incident energy. Values of $a_2=0.598$ and $a_3=0.408$ were found to provide a good description of the light response of the detectors. It should be noted that the coefficients a_0 and a_1 extracted from the analysis are not only dependent on the detector response, but also that of the electronic processing.

III. RESULTS

The ^{4}He, ^{6}He, and ^{8}He reaction products were identified from their characteristic energy-loss in the Si-CsI telescopes. A particle identification spectrum is shown in Fig. 1. The loci corresponding to the four particle-bound helium isotopes are clearly identified, thus permitting the breakup channels to be selected cleanly. Using the measurements of the mass, energy, and emission angle of the fragments, the energy of the undetected recoil was calculated via momentum conservation, and the various reaction Q values reconstructed.

A. The ^{12}C(^{12}Be,^{4}He,^{6}He)^{14}C and reaction

The Q-value spectra for the ^{12}C(^{12}Be,^{4}He,^{6}He)^{14}C reaction [$Q=+2.04$ MeV] is shown in Fig. 2 for (a) the ^{nat}C

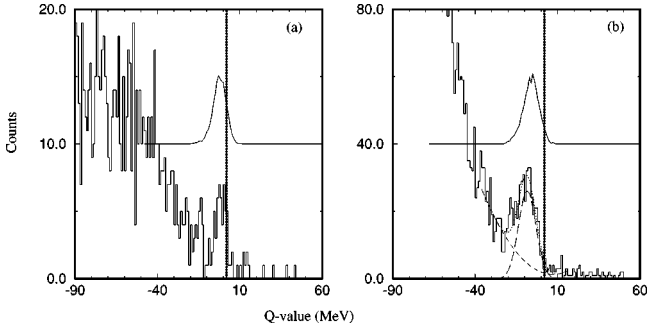

FIG. 2. The Q-value spectra for the ^{12}C(^{12}Be,^{4}He,^{6}He)^{14}C reaction, for (a) the natural carbon target and (b) the $(CH_2)_n$ target. The vertical lines indicate the expected ground state Q value. A fit to the experimental data with a Gaussian form is shown in (b). The solid lines show the Monte Carlo calculations of the ^{12}C(^{12}Be,^{4}He,^{6}He)^{14}C reaction for the two targets.

target and (b) the $(CH_2)_n$ target. The vertical dotted line shows the predicted location of the peak corresponding to the production of all of the final state nuclei in their ground states, a peak appears in these spectra close to the predicted Q value. The differences in the location in the Q-value peaks for the two targets is due, in part, to differences in the energy losses of the beam and reaction products in the two targets. The experimental Q-value resolutions are 9.0 and 12.5 MeV (FWHM), respectively, for the two targets. Monte Carlo simulations of the reaction and detection processes, which include the beam energy and angular resolutions and the energy and position resolutions of the detectors, indicate that the Q-value resolution should be 9 and 12 MeV (FWHM). This is in good agreement with the experimental data. In addition, the simulations describe the shift in the peak energies between the two targets. With this resolution it is not possible to resolve possible excitations of the ^{14}C recoil nucleus.

The above Monte Carlo calculations suggest that the detection efficiency for the ^{12}C(^{12}Be,^{4}He,^{6}He)^{14}C reaction was $\sim$45%. In these simulations it was assumed that the two neutron transfer cross section could be approximated by an exponential dependence given by

$$\frac{d\sigma}{d\Omega} \propto \exp(-\theta_{\mathrm{c.m.}}/12), \tag{2}$$

where $\theta_{\mathrm{c.m.}}$ is the center-of-mass angle. The angular distributions in the ^{10}Be decay frame were assumed to be isotropic. The angular dependence of the differential cross section for the ^{12}C(^{12}Be,^{10}Be)^{14}C reaction is unknown, but exponential fall-off factors of 12 to 16 are typical for such reactions (see, for example, Ref. [24]). In addition, the reaction yield in the present measurement is forward peaked with a decrease in angle which is in accord with Eq. (2). Varying the fall-off factor scales the detection efficiency: for example an increase or decrease by a factor of 2 results in detection efficiencies of 30 and 55 %, respectively. Assuming a 40% detection efficiency, the cross section for the two neutron stripping reaction leading to α unbound states in ^{10}Be is 0.22 ± 0.06 mb for the $^{\mathrm{nat}}$C target and 0.29 ± 0.05 mb for the $(CH_2)_n$ target. The uncertainties are statistical and do not include the systematic uncertainties in the target thickness and those arising from the simulated detection efficiency. These two measurements agree within the statistical errors.

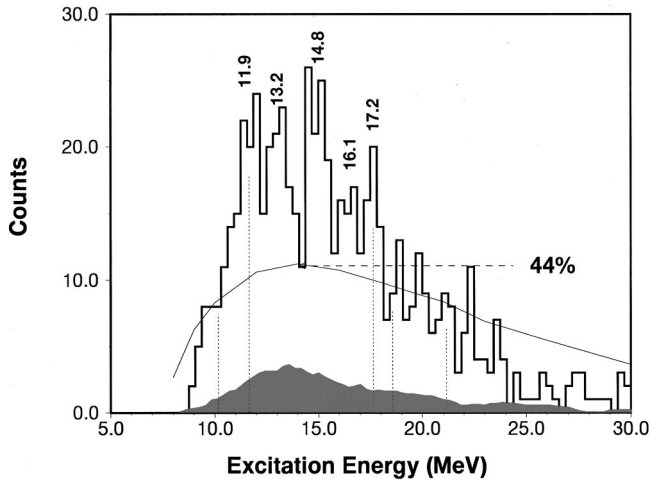

FIG. 3. The ^{10}Be excitation energy spectrum. The solid line is the simulated detection efficiency (peaking at 44%), and the vertical dotted lines indicate the energies of known states in this nucleus.

The excitation energy of the ^{10}Be nucleus can be calculated from the relative velocities of the ^{4}He and ^{6}He nuclei, as determined from the measurement of the energies and emission angles of the fragments. Figure 3 shows the ^{10}Be excitation energy spectrum gated on the Q-value peaks in Figs. 2(a) and 2(b). The spectrum spans the excitation energy range from 9 to 25 MeV. The envelope of these data is reasonably well described by the simulated detection efficiency (solid line). Also shown in this figure is the background contribution to this spectrum calculated by placing a gate just below the peak in Fig. 2(b). The width of the gate was adjusted so that it included the same number of counts as deduced from the fit to the peak in the same spectrum. The bulk of the yield in the excitation energy spectrum is thus associated with the decay of states in ^{10}Be. The vertical dotted lines in Fig. 3 indicate the energies of states previous known in this nucleus [25], and there appears to be good agreement with the present data. The yield between 11.9 and 17.2 MeV must thus be associated with previously untabulated states in this nucleus. Hence, the peaks at 13.2, 14.8, and 16.1 MeV provide evidence for three new states in ^{10}Be. The statistical uncertainty on the excitation energies is 0.4 MeV, whilst the systematic uncertainty on the absolute energies is 0.5 MeV. The systematic error in differences in excitation energies is significantly smaller than the statistical error ($\sim$100 keV).

The widths of the above peaks are $\sim$1 MeV, which is larger than the calculated 500 keV estimated by the Monte Carlo simulations. This may suggest that either the states are intrinsically broad or are unresolved multiplets. Known states in ^{10}Be in this excitation energy region typically have widths from 100 to 350 keV, suggesting that this measure-

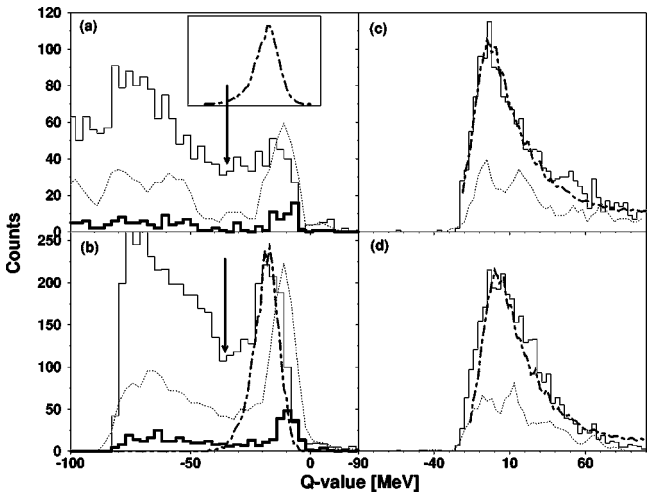

FIG. 4. *Q*-value spectra for the reactions (a) ^{12}C(^{12}Be,^{6}He,^{6}He), (b) ^{12}C(^{12}Be,^{4}He,^{8}He), (c) p(^{12}Be,^{6}He,^{6}He), and (d) p(^{12}Be,^{4}He,^{8}He) from the $(CH_2)_n$ target. The arrows indicate the *Q*-value cutoff used to discriminate between the two target components. The bold histograms in (a) and (b) are for the reactions from the ^{nat}C target. The dotted curves in (a) to (d) correspond to the ^{nat}C target data scaled to account for differences in beam exposure and thickness of the two targets, and in (c) and (d) indicates the level of background in these spectra. The dot-dash curves in (c) and (d) represent the results of Monte Carlo simulations of the reactions from the proton target. The inset in (a) and the dot-dashed line in (b) show the results of the simulation of the ^{12}C(^{12}Be,^{6}He,^{6}He) and ^{12}C(^{12}Be,^{4}He,^{8}He) reactions for the $(CH_2)_n$ target.

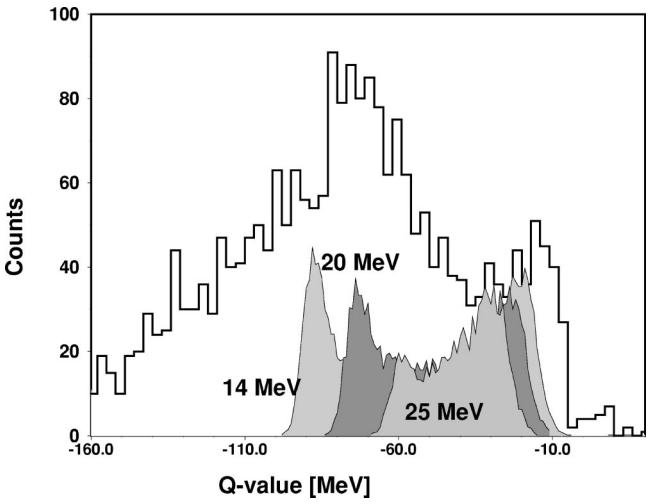

FIG. 5. Monte Carlo simulations of the p(^{12}Be,^{6}He,^{6}He) reaction with ^{12}Be excitation energies of 14, 20, and 25 MeV, reconstructed assuming a ^{12}C recoil.

ment is not measuring the natural widths of the states but is dominated by either the experimental resolution or contributions from several states.

B. ^{12}Be breakup reactions

Figures 4(a) and 4(b) show the *Q*-value spectrum reconstructed for ^{6}He+^{6}He and ^{8}He+^{4}He coincidences assuming the reactions ^{12}C(^{12}Be,^{6}He,^{6}He) [$Q=-10.1$ MeV] and ^{12}C(^{12}Be,^{8}He,^{4}He) [$Q=-8.9$ MeV], respectively (previously presented in Ref. [20]). The bold histogram corresponds to reactions from the natural carbon target (denoted ^{nat}C), and the narrow-lined histogram corresponds to reactions from the $(CH_2)_n$ target, assuming a ^{12}C recoil. The peaks in the spectra at $Q\simeq-10$ MeV indicate that the two reactions have been correctly identified. The inset in Fig. 4(a) and the dot-dashed line in Fig. 4(b) display the result of Monte Carlo simulations of the reaction processes for the $(CH_2)_n$ target. As before, these simulations include the effects of the position and energy resolutions of the detectors, energy and angular spread of the beam and energy and angular straggling of the beam and reaction products in the target. The simulations agree well with the reconstructed peak energy for the ^{4}He+^{8}He and ^{6}He+^{6}He channels confirming the origin of the data, and the calculated *Q*-value resolution are 11.5 MeV for the $(CH_2)_n$ target. The experimental widths, however, appears to be closer to 15 MeV. Given that the simulations reproduce the 9 MeV resolution of the ^{nat}C target data, this feature indicates that there is a further contribution from reactions on the hydrogen component, causing it to be broader. In order to determine the contribution of reactions from the protons in the $(CH_2)_n$ target, the ^{nat}C target data have been scaled in accordance with the known ^{nat}C areal densities [the dotted line, in Figs. 4(a) and 4(b)]. This demonstrates that the peaks in these spectra are predominantly accounted for by reactions from the ^{12}C component of the target, but in the region just below the peaks there is an additional contribution, and the *background* yield ($Q<-40$ MeV) is significantly enhanced compared to the natural carbon target data.

Figure 5 shows the *Q*-value spectrum for the $(CH_2)_n$ target [from Fig. 4(a)] compared with Monte Carlo simulations of the p(^{12}Be,^{6}He,^{6}He) reaction, for various ^{12}Be excitation energies, but reconstructed assuming a ^{12}C recoil. This comparison demonstrates that the broad bump in the *Q*-value spectrum at $Q\simeq-70$ MeV is associated with reactions in which the recoil protons are emitted at large center-of-mass angles and does not originate from background processes. The simulations also show that the proton recoil data extend into the region close to the peak identified with the ^{12}C(^{12}Be,^{6}He,^{6}He) reaction, and that the reactions from the proton and ^{12}C components of the $(CH_2)_n$ target are not completely resolved.

Figure 4(c) shows the data for the $(CH_2)_n$ target in Fig. 4(a) reconstructed assuming the reaction p(^{12}Be,^{6}He,^{6}He); in the instance that an event was associated with the peak at $Q\simeq-10$ MeV in Fig. 4(a), the spectrum in Fig. 4(c) was not incremented. The cutoff point in the *Q*-value spectrum employed in the analysis is shown by the arrow in Fig. 4(a). The dotted line in Fig. 4(c) again shows the scaled ^{nat}C target data, suggesting that the background contribution to the *Q*-value spectrum is of the order of 20 to 30 %, further demonstrating that this spectrum is dominated by events from the p(^{12}Be,^{6}He,^{6}He) reaction. The bold dot-dash line in Fig. 4(c) displays the results of Monte Carlo simulations for the p(^{12}Be,^{6}He,^{6}He) reaction, normalized to the data and corrected for the background contribution. The simulations

reproduce the shape of the spectrum, including the high-energy tail. The poorer resolution (26 MeV) is due to the larger recoil energy carried away by the protons, which is less well reconstructed than for the lower energy ^{12}C recoils. Figure 4(d) displays the results of a similar analysis for the ^{4}He+^{8}He coincidences assuming the $p(^{12}\mathrm{Be},{}^{4}\mathrm{He},{}^{8}\mathrm{He})$ reaction ($Q=-8.9$ MeV). Figures 4(b) and 4(d) demonstrate that ^{4}He+^{8}He coincidences arise from the breakup of ^{12}Be produced in reactions from both ^{12}C and protons.

Assuming that the angular distributions for the two reactions $p,{}^{12}\mathrm{C}({}^{12}\mathrm{Be},{}^{12}\mathrm{Be}^{*})$ can be described by Eq. (2) (The exponential fall-off factor of 12° is taken from the measurements of Ref. [21]), then the Monte Carlo simulations suggest that the detection efficiency is ~40%. To provide an estimate of the sensitivity to the nature of the primary angular distributions, it may be noted that an isotropic distribution gives an efficiency of 25%. The efficiency may be used to calculate the total ^{6}He+^{6}He breakup cross section for reactions from both the proton and carbon targets. The cross sections for the $^{12}\mathrm{C}({}^{12}\mathrm{Be},{}^{6}\mathrm{He},{}^{6}\mathrm{He})$ reaction from the natural carbon and $(CH_2)_n$ targets are deduced to be 0.28 ± 0.04 mb and 0.14 ± 0.06 mb, respectively, the disagreement here is not statistically significant. For the reactions from the proton component of the $(CH_2)_n$ target the reaction cross section is 0.41 ± 0.03 mb, suggesting that the reaction cross section is slightly larger in the case of the proton target. Similarly, the cross section for the $^{12}\mathrm{C}({}^{12}\mathrm{Be},{}^{8}\mathrm{He},{}^{4}\mathrm{He})$ reaction from the natural carbon and $(CH_2)_n$ targets are calculated to be 0.79 ± 0.07 mb and 0.86 ± 0.04 mb, respectively, demonstrating good agreement.

The excitation energy of the ^{12}Be nuclei prior to decay has been calculated from the relative velocity of the two breakup fragments. The spectrum shown in Fig. 6(a) corresponds to the combined data from both targets for the ^{6}He+^{6}He breakup channel (previously shown in Ref. [20]). Peaks are observed in this spectrum at the energies listed in Table I. The spins assigned to the peaks are those deduced from the angular correlation analysis reported in [20]. Figure 7 displays the angular distributions of the reconstructed ^{12}Be reaction products for the $p(^{12}\mathrm{Be},{}^{12}\mathrm{Be}^{*})$ reaction over the center-of-mass angular interval for which it was possible to separate the reactions from the two targets. The angular distributions are shown for the three peaks in the excitation energy spectrum for which spin assignments have been suggested, namely, 13.2 MeV (4^+), 16.1 MeV (6^+), and 20.9 MeV (8^+). The three distributions have been corrected for the variation of detection efficiency with scattering angle, and have been scaled so that they can be displayed simultaneously. Two features are evident: first the shape of the distributions for the lowest energy state is different from that of the two other states, and secondly these latter two states are backward peaked. The difference in the shape of the distributions would confirm that the 13.2 MeV state does indeed have a different spin from that of the other two. On the other hand, due to the similarity of the distributions for the 16.1 and 20.9 MeV states it is not possible to confirm the different spins extracted from the angular correlation analysis. However, it is known that reactions leading to higher spin particles in the final state, and with mismatched entrance and exit channel angular momenta, exhibit very similar angular distributions [26].

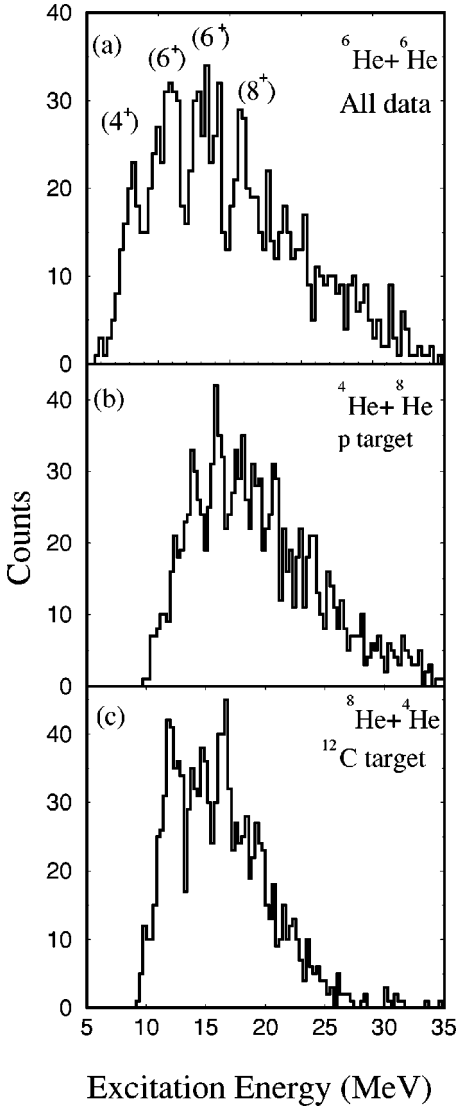

FIG. 6. The ^{12}Be excitation energy spectrum for (a) ^{6}He+^{6}He decays for the proton and carbon targets combined; (b) ^{4}He+^{8}He decays for proton recoils for $\theta_{\mathrm{c.m.}}>100°$ and (c) ^{4}He and ^{8}He decays for ^{12}C recoils.

The observation of the reactions from the proton target with backward peaked angular distributions has led to a reanalysis of the ^{4}He+^{8}He breakup data presented in Ref. [20]. Originally, it was not possible to resolve excited states in the $p(^{12}\mathrm{Be},{}^{4}\mathrm{He}+{}^{8}\mathrm{He})$ reaction. However, peaks are observed in the ^{12}Be excitation energy spectrum, for ^{4}He+^{8}He decays for both the ^{12}C and proton targets, if in the latter case the center-of-mass emission angles are limited such that $\theta_{\mathrm{c.m.}}>100°$ [Figure 6(b)].

The spectrum for the proton target data now shows evidence for a series of peaks that was absent in the earlier analysis. The energies of these are given in Table II. Interestingly, there seems to be a reasonable correlation with the higher energy states observed in the ^{6}He+^{6}He decay channel. The peak at 16.0 MeV is observed in both channels, the

TABLE I. Excitation energies and spins for the ^{6}He+^{6}He breakup states.

^{6}He+^{6}He	E_x [MeV]	13.2	14.9	16.1	17.8	18.6	19.3	20.9	22.8	(24.0)	(25.1)
	J	4		6		6		8			

triplet of states at 17.8, 18.6, and 19.3 MeV are correlated with a triplet at 17.4, 18.2, and 19.4 MeV, and finally the strong peak at 20.9 MeV in the ^{6}He+^{6}He decay channel has a counterpart at 20.7 MeV. There are, however, differences at lower excitation energies; most notably the appearance of a peak at 14.1 MeV in the ^{8}He+^{4}He decay channel, the absence of which in the ^{6}He+^{6}He decay spectrum may indicate a state with negative parity. The spectrum of states observed in the ^{4}He decay channel following ^{12}Be reactions with the ^{12}C target again indicates the presence of the 14.1 MeV state but the peak at 16.0 MeV in the proton target data now appears with at 16.5 MeV. These differences indicate that the spectrum of states is perhaps more complicated than revealed in the present measurements and points to the need for much higher resolution studies.

IV. DISCUSSION

A. ^{10}Be

A number of states in ^{10}Be have been seen to be strongly excited in the ^{9}Be$(d,p)^{10}$Be [27] and ^{9}Be$(\alpha,^{3}$He$)^{10}$Be [28] reactions. Predominantly, it is the ground state band 0.0 MeV (0^+), 3.368 (2^+), and $\sim$10.4 MeV ([4^+]) and rotational states associated with the 1^- 5.960 MeV state [6.263 MeV (2^-), 7.371 MeV (3^-), 9.27 MeV (4^-), and 11.76 MeV ([5^-])] that are populated. The assignment of the 5^- member of the 1^- band is based on spin-energy systematics [18], i.e., the extrapolation of the 1^- band. The strong population of these two bands may be linked to their structure. The ^{9}Be nucleus possesses a single valence neutron in the $1p_{3/2}$ orbit and the neutron transferred in the above reactions can either occupy the vacancy in this orbit or those in the $1p_{1/2}$, $2s_{1/2}$, and $1d_{5/2}$ levels. The ^{10}Be ground state configuration would then correspond to the transfer of a neutron into the $1p_{3/2}$ orbit. The molecular-orbital model calculations [14,15] suggest that the 1^- state may be associated with the $1p_{3/2}$ neutron coupled to a neutron in the prolate aligned $1d_{5/2}$ orbit which may be associated with the Nilsson quantum numbers $[220]1/2^+$. It is this configuration which is believed to produce the pronounced molecular structure. In the molecular-orbital model the deformation arising from the $\alpha+\alpha$ cluster core is calculated to be sufficient to lower the energy of this level such that it lies below the $1p_{1/2}$ level, and is responsible for the low-lying $1/2^+$ (1.68 MeV) in ^{9}Be. Seya *et al.* [15] also suggest that there should be two other molecularlike configurations in this nucleus corresponding to the neutron configurations $(1p_{3/2}\otimes 1p_{1/2})$ $[2^+]$ and $([220]1/2^+)^2$ $[0_2^+]$, associated with the states at 5.958 and 6.179 MeV, respectively. These states are not observed in the neutron transfer reactions. This description is supported by the recent theoretical studies using the molecular orbit [29] and AMD [30] frameworks.

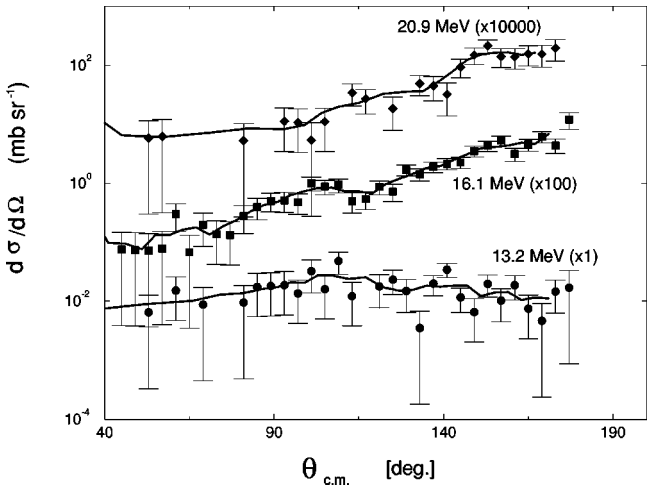

FIG. 7. Angular distributions for the $p(^{12}$Be,^{12}Be*) reaction for ^{6}He+^{6}He decays for the 13.2 MeV (4^+), 16.1 MeV (6^+), and 20.9 MeV (8^+) states. The angular distributions have been corrected for the varying detection efficiency as a function of the center-of-mass scattering angle. The solid lines are to guide the eye.

A study by Hamada *et al.* [31] of the ^{7}Li$(\alpha,p)^{10}$Be, ^{3}H-transfer reaction revealed evidence for the excitation of the 0_2^+ band, with the 7.542 (2^+) state being observed together with a possible 4^+ state at either 10.2 or 10.57 MeV. In the same reaction, the 1^- band was observed up to the 5^- candidate at 11.76 MeV. Large cluster spectroscopic factors were measured for these states, but in this instance ^{7}Li+t clusters were assumed. Recently, Soić *et al.* [22] undertook a search for ^{4}He+^{6}He break-up of ^{10}Be using the ^{7}Li$(^{7}$Li,α^{6}He$)\alpha$ reaction. A comparison between the ^{4}He +^{6}He and $n+^{9}$Be decay channels suggested that the 10.2 MeV state decayed strongly by α-emission and was absent in the neutron-decay channel, while the opposite was true for the 10.57 MeV state. This latter information may indicate that the 10.2 MeV state is molecular in nature and the 10.57 MeV state is the 4^+ member of the ground state band. Finally, the α-spectrocopic factors for the 7.371 MeV (3^-) and 7.542 MeV (2^+) states, measured by Milin *et al.* [32], suggests that these states may have a well developed ^{4}He +^{6}He cluster structure.

Due to the limited resolution and decreasing detection efficiency close to the barrier of the present measurement, we are not able to observe the 10.2 MeV state. However, as noted above we do find evidence for three new states at 13.2,

TABLE II. Excitation energies for ^{8}He+^{4}He breakup states, from the ^{nat}C and proton targets.

^{12}C target	E_x [MeV]	12.1	14.1	15.1	16.5				
^{1}H target	E_x [MeV]		14.1		16.0	17.4	18.2	19.4	20.7

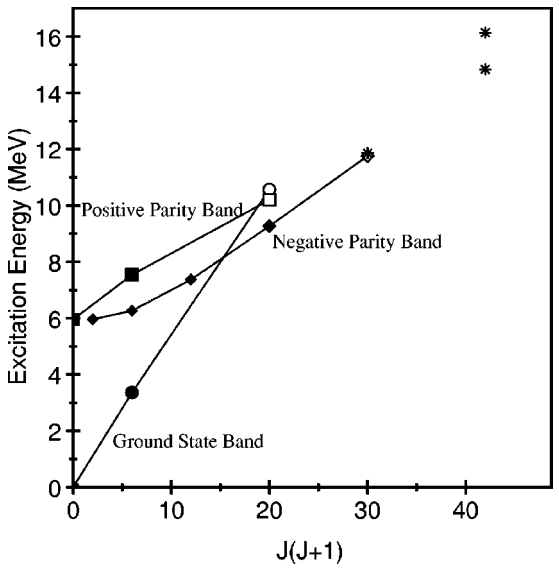

FIG. 8. The energy-spin systematics for states in ^{10}Be. Filled symbols are states with measured spins, open symbols are the suggested spins from Ref. [18], and the stars correspond to the states observed in the present work (see the text for details).

14.8, and 16.1 MeV which decay into ^{4}He+^{6}He. Based upon the evidence of Soić *et al.* [22] and Milin *et al.* [32], these three states might be the continuation of the 0^+ and 1^- rotational bands. Extrapolating from the existing energy-spin systematics, the 6^+ member of the 0^+ band would lie at approximately 15.3 MeV. Two of the present states lie close to this energy (16.1 and 14.8 MeV) and hence may be the extension of this band. Further, we also observe a state at 11.9 MeV, close to the predicted 11.76, 5^- member of the negative parity band (see Fig. 8). We note that due to parity selection rules, the present study cannot observe unnatural parity states, and thus the 6^- state would be absent from the spectrum in Fig. 3. However, it is not possible to account for the multiplicity of states observed in the present measurement by above rotational bands, and thus the structure of ^{10}Be, as revealed by α decay, must be more complex.

The ground state of the ^{12}Be projectile might be expected to have a closed $1p$ shell for the neutrons [33–35], and hence a simple stripping reaction would not populate the molecular bands apart from those that are built on the $1p_{3/2} \otimes 1p_{1/2}$ (2^+) configuration. However, spd-shell model calculations [36,37] and a recent measurement of high-energy ^{12}Be one-neutron knockout experiments [38] indicate that only $\sim$30% of the ^{12}Be ground state wave function corresponds to the closed neutron shell, and that there are significant contributions from configurations in which a pair of neutrons occupy orbits in the sd shell. An analysis of the Coulomb energies of the nuclei ^{12}O and ^{12}Be by Sherr and Fortune [39] similarly suggests that the ^{12}Be ground state contains a $\sim$50% contribution from the $^{10}\mathrm{Be}_{\mathrm{g.s.}} \otimes (2s_{1/2})^2$ configuration, as originally postulated by Barker [33]. These components would then allow access to the molecular-bands through a $2n$ stripping reaction.

TABLE III. $p+^{12}$Be optical model parameters used in the coupled channel analysis.

V_R	r_R	a_R	W_S	r_S	a_S	r_C
16.27 MeV	1.48 fm	0.61 fm	5.05 MeV	1.20 fm	0.14 fm	1.25 fm

B. ^{12}Be

In order to attempt to reproduce the angular distributions for the $p(^{12}\mathrm{Be},^{12}\mathrm{Be}^*)$ reaction (Fig. 7), we have performed coupled channels calculations of the $p+^{12}$Be reaction using the CHUCK99 code [40]. The excitation process has been modeled assuming that there are two rotational bands: the ground state band, the deformation of which is given by the energy of the 2.1 MeV 2^+ state, and which is assumed to have members extending to a spin of 6^+; and a second band with a moment of inertia given by the energy-spin characteristics reported in Ref. [20] [i.e., $E_0 = 10.8(\pm 1.8)$ MeV, $\hbar^2/2\mathcal{I} = 0.15(\pm 0.04)$ MeV], and which extends up to a spin of 8^+. The two bands were coupled by means of $E2$ excitations, both in band and interband, while also allowing for reorientation. The optical model potentials were taken from the studies of $p+^{12}$Be elastic scattering at 55 MeV per nucleon [21], and are shown in Table III. The results of these calculations for the 4^+ to 8^+ states in the excited band are shown in Fig. 9. The left hand panel displays the differential cross sections and the right hand panel the channel-spin decomposition of the cross section. The calculations, as with the experimental data, show that the cross sections depend only weakly on the center-of-mass angle. However, the calculations do not reproduce the observed experimental trends in detail. It is noticeable that the cross sections for populating the excited states depends strongly on the spin, and in any case are considerably smaller than those observed experimentally. The shape of the $J=4$ angular distribution does not agree with the experimental data, on the other hand there

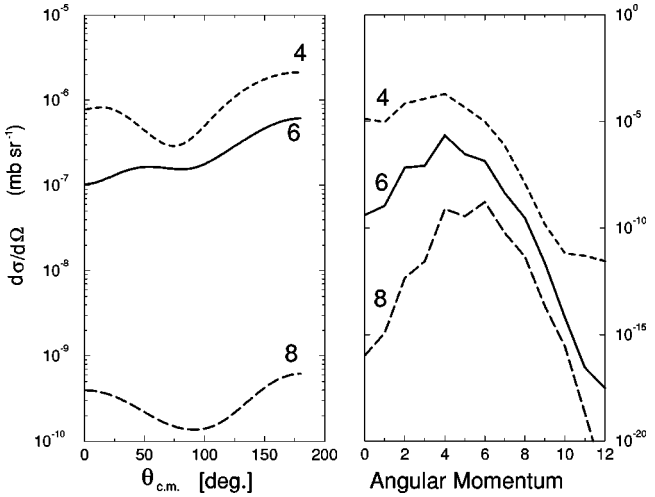

FIG. 9. Coupled channel calculations of the $p(^{12}\mathrm{Be},^{12}\mathrm{Be}^*)$ reaction for the 13.2 MeV (4^+), 16.1 MeV (6^+), and 20.9 MeV (8^+) states. The left hand panel shows the differential cross sections and the right hand panel the associated channel-spin decomposition.

is better agreement for the suggested $J=6$ and 8 states, indeed the calculations show a very similar backward angle behavior. Moreover, the angular distributions for $J=4$ are different from those for $J=6$ and 8, and this would further strengthen the earlier spin assignments.

The lack of agreement between the experimental and theoretical distributions, both in terms of overall magnitude and shape, may arise for two reasons. First, it is possible that the cross sections observed experimentally are much larger than their theoretical counterparts due to the over simplification of the predicted excitation mechanism, whereas the excitation process may be much more complex. For example, the small neutron binding energy might suggest that coupling to one- and two-neutron transfer channels could be important. In addition, it is likely that the potentials used to describe the $p+{}^{12}$Be interaction are inappropriate as they have been assumed to be energy-independent. The partial wave decompositions, shown in Fig. 8, peak around angular momenta of 4 to 6 $\hbar$, whereas the analysis of the angular correlations in Ref. [20] indicated that the grazing angular momentum lies around 6 to 7 $\hbar$.[1] Elastic scattering measurements over the energy range of present interest would help resolve this discrepancy.

V. CONCLUSIONS

A measurement of the ^{12}C(^{12}Be,^{4}He,^{6}He) reaction has found evidence for three new states in ^{10}Be at 13.2, 14.8, and 16.1 MeV that decay by α emission. It is suggested that these states are linked with the continuation of the 0_2^+ molecular band in this nucleus. An analysis of angular distributions of ^{6}He+^{6}He coincidences produced from the decay of ^{12}Be, excited in the p(^{12}Be,^{6}He,^{6}He) reaction, indicates that the reaction yields depend only weakly on scattering angle. This is consistent with the angular distributions calculated using the coupled channels approach. The coupled channel calculations are, however, unable to reproduce the magnitudes of the reaction cross sections. The reconstruction of the ^{4}He+^{8}He coincidences from the reaction p(^{12}Be,^{8}He,^{4}He), limited to backward emission angles, provides evidence for states in ^{12}Be many of which are found to be correlated with those in the ^{6}He+^{6}He decay channel. It is possible that these ^{12}Be excited states form part of an excited molecular band. However, the strongest evidence for the molecular nature of the states reported here would be large cluster spectroscopic factors. Hence, more detailed measurements of the partial decay widths and spins of the observed states observed in the present measurement would be help confirm this link.

[1] We note that there was an error in the calculation of the theoretical grazing angular momentum given in Ref. [20].

ACKNOWLEDGMENTS

The authors are grateful to the technical and operations staff of LPC and GANIL: in particular J. M. Gautier, P. Derues, D. Etasse, P. Le Saec, J. Tiller, and J. M. Fortbonne. This work was funded by the EPSRC (U.K.) and the IN2P3-CNRS (France). Additional support was provided by the ALLIANCE program of the British Council and the Ministère des Affaires Etrangères, and the Human Capital and Mobility Program of the European Community (Contract No. CHGE-CT94-0056).

[1] D. M. Brink, *Proceedings of International School ''Enrico Fermi,''* No. 36, Varenna, 1965 (Academic, New York, 1966), p. 247.
[2] D. M. Brink, Nucl. Phys. **A91**, 1 (1967).
[3] J. Zhang and W. D. M. Rae, Nucl. Phys. **A564**, 252 (1993).
[4] J. Zhang, W. D. M. Rae, and A. C. Merchant, Nucl. Phys. **A575**, 61 (1994).
[5] Y. Kanada-En'yo, H. Horiuchi, and A. Doté, J. Phys. G **24**, 1499 (1998).
[6] A. Doté, H. Horiuchi, and Y. Kanada-En'yo, Phys. Rev. C **56**, 1844 (1997).
[7] Y. Kanada-En'yo and H. Horiuchi, Phys. Rev. C **52**, 628 (1995).
[8] H. Horiuchi and Y. Kanada-En'yo, Nucl. Phys. **A616**, 394c (1997).
[9] A. Doté, H. Horiuchi, and Y. Kanada-En'yo, Phys. Rev. C **56**, 1844 (1997).
[10] D. Baye and P. Descouvemont, in *Proceedings of the 5th International Conference on Clustering Aspects in Nuclear and Subnuclear Systems*, Kyoto, Japan, 1988 [J. Phys. Soc. Jpn. **58**, 103 (1989)].
[11] P. Descouvemont, Phys. Rev. C **44**, 306 (1991).
[12] M. Dufour and P. Descouvemont, Nucl. Phys. **A605**, 160 (1996).
[13] M. Dufour and P. Descouvemont, Phys. Rev. C **56**, 1831 (1997).
[14] S. Okabe and Y. Abe, Prog. Theor. Phys. **61**, 1049 (1971).
[15] M. Seya, M. Kohno, and S. Nagata, Prog. Theor. Phys. **65**, 204 (1981).
[16] J. M. Eisenberg and W. Greiner, *Nuclear Theory 1* (North Holland, Amsterdam, 1975), p. 571.
[17] W. von Oertzen, Z. Phys. A **354**, 37 (1996).
[18] W. von Oertzen, Z. Phys. A **357**, 355 (1997).
[19] W. von Oertzen, Nuovo Cimento **110**, 895 (1997).
[20] M. Freer *et al.*, Phys. Rev. Lett. **82**, 1383 (1999).
[21] A. A. Korsheninnikov *et al.*, Phys. Lett. B **343**, 53 (1995); RIKEN Report No. AF-NP-175, 1994.
[22] N. Soić *et al.*, Europhys. Lett. **34**, 7 (1996).
[23] D. Horn *et al.*, Nucl. Instrum. Methods Phys. Res. A **320**, 273 (1992).
[24] H. G. Bohlen *et al.*, Z. Phys. A **308**, 121 (1982).
[25] F. Ajzenberg-Selove, Nucl. Phys. **A490**, 1 (1988).
[26] G. R. Stachler, in *Direct Nuclear Reactions, International Series of Monographs on Physics*, edited by R. J. Elliot, J. A. Krumhansl, and D. H. Wilkinson (Oxford Science, Oxford, 1983), p. 556.
[27] R. E. Anderson, J. J. Kraushaar, M. E. Rickey, and W. Zim-

merman, Nucl. Phys. **A236**, 77 (1974).
[28] M. N. Harakeh, J. van Popta, A. Saha, and R. H. Siemssen, Nucl. Phys. **A344**, 15 (1980).
[29] N. Itagaki and S. Okabe, Phys. Rev. C **61**, 044306 (2000).
[30] Y. Kanada-En'yo, H. Horiuchi, and A. Doté, Phys. Rev. C **60**, 064304 (1999).
[31] S. Hamada, H. Yasue, S. Kubonos, M. H. Tanaka, and R. J. Peterson, Phys. Rev. C **49**, 3192 (1994).
[32] M. Milin *et al.*, Europhys. Lett. **48**, 616 (1999).
[33] F. C. Barker, J. Phys. G **2**, L45 (1976).
[34] H. T. Fortune, G. B. Liu, and D. E. Alburger, Phys. Rev. C **50**, 1355 (1994).
[35] T. Suzuki and T. Otsuka, Phys. Rev. C **56**, 847 (1997).
[36] E. K. Warburton and B. A. Brown, Phys. Rev. C **46**, 923 (1992).
[37] B. A. Brown (private communication).
[38] A. Navin *et al.*, MSU report, 1999 (unpublished).
[39] R. Sherr and H. T. Fortune, Phys. Rev. C **60**, 064323 (1999).
[40] N. M. Clarke, CHUCK99 version, University of Birmingham, derived from CHUCK (P. D. Kunz) and CHUCK3 (J. R. Comfort).